GDCh Communications Angewandte Chemie International Edition www.angewandte.org

How to cite: *Angew. Chem. Int. Ed.* **2023**, *62*, e202311519
doi.org/10.1002/anie.202311519

CN$_3$ Ions **Hot Paper**

Stabilization of Guanidinate Anions $[CN_3]^{5-}$ in Calcite-Type $SbCN_3$

*Lukas Brüning, Nityasagar Jena, Elena Bykova, Pascal L. Jurzick, Niko T. Flosbach, Mohamed Mezouar, Michael Hanfland, Nico Giordano, Timofey Fedotenko, Björn Winkler, Igor A. Abrikosov, and Maxim Bykov**

Abstract: The stabilization of nitrogen-rich phases presents a significant chemical challenge due to the inherent stability of the dinitrogen molecule. This stabilization can be achieved by utilizing strong covalent bonds in complex anions with carbon, such as cyanide CN^- and NCN^{2-} carbodiimide, while more nitrogen-rich carbonitrides are hitherto unknown. Following a rational chemical design approach, we synthesized antimony guanidinate $SbCN_3$ at pressures of 32–38 GPa using various synthetic routes in laser-heated diamond anvil cells. $SbCN_3$, which is isostructural to calcite $CaCO_3$, can be recovered under ambient conditions. Its structure contains the previously elusive guanidinate anion $[CN_3]^{5-}$, marking a fundamental milestone in carbonitride chemistry. The crystal structure of $SbCN_3$ was solved and refined from synchrotron single-crystal X-ray diffraction data and was fully corroborated by theoretical calculations, which also predict that $SbCN_3$ has a direct band gap with the value of 2.20 eV. This study opens a straightforward route to the entire new family of inorganic nitridocarbonates.

The search for novel synthetic routes to solid-state nitrides is important due to the broad range of potential applications for these materials.[1,2] However, the synthesis of N-based materials is challenging due to the stability of dinitrogen molecule and therefore nitrides are significantly outnumbered by other classes of compounds.[3] Among various synthesis methods, like self-propagating combustion reactions, ammonolysis, solid-state metathesis,[1,2] high-pressure techniques provide unique opportunity to achieve compounds with very high nitrogen content, as corroborated by previous studies on polynitrides.[4–11] While high-pressure synthetic routes to binary nitrides using laser-heated diamond anvil cells (DACs) are relatively well established, one of the remaining fundamental challenges of the high-pressure chemistry is to explore routes to stable ternary nitrogen-rich nitrides. This challenge can be addressed by utilizing strong covalent bonding in complex anions with carbon as well as the diversity of possible hybridizations of carbon and nitrogen atoms. Ternary compounds containing carbon and nitrogen such as cyanides $[CN]^-$ and carbodiimides $[CN_2]^{2-}$ have been known for a long time.[12] Further extending the series we can envision guanidinates $[CN_3]^{5-}$ and ortho-nitridocarbonates $[CN_4]^{8-}$, analogous to carbonates $[CO_3]^{2-}$ and orthocarbonates $[CO_4]^{4-}$.[13–15]

A straightforward approach to synthesizing guanidinates involves the deprotonation of guanidine, which can be performed by strong bases like alkali metal hydrides or amides (Table S1).[16–24] This method allowed achieving the double-deprotonated guanidinates with the chemical formula $MC(NH)_3$ (M=Ca, Ba, Sr, Eu, Yb).[17,20,24,25] However, achieving full deprotonation of guanidine proves impossible due to guanidine‘s inherent properties as a very strong base itself.

Recently Dronskowski et al. predicted a synthetic route to completely deprotonated guanidinates of group 5 metals (VCN_3, $NbCN_3$, $TaCN_3$). The metathetic pathway utilizes reactions between metal pentachlorides (MCl_5) with sodium carbodiimide and high-energy sodium nitride.[26] These compounds are predicted to be thermodynamically unstable due to the existence of the very stable metal nitrides like Ta_2N_3, VN and NbN.[4,27,28] Although the suggested metathetic route is exothermic and group 5 guanidinates can therefore be kinetically stabilized, this synthesis is extremely challenging to realize at high-pressure conditions in laser-heated diamond anvil cells due to the small sample size and its inhomogeneity. The advantage of the DAC method, however, is the

---

[*] L. Brüning, P. L. Jurzick, N. T. Flosbach, Dr. M. Bykov
Institute for inorganic Chemistry,
University of Cologne
50939, Cologne (Germany)
E-mail: maxim.bykov@uni-koeln.de

Dr. N. Jena, Prof. I. A. Abrikosov
Department of Physics, Chemistry and Biology (IFM),
Linköping University,
Linköping SE-58183 (Sweden)

Dr. E. Bykova, Prof. B. Winkler
Institute of Geosciences,
Goethe University Frankfurt,
60438 Frankfurt (Germany)

Dr. M. Mezouar, Dr. M. Hanfland
European Synchrotron Radiation Facility,
Grenoble Cedex F-38043 (France)

Dr. N. Giordano, Dr. T. Fedotenko
Deutsches Elektronen-Synchrotron (DESY)
22607 Hamburg, (Germany)

possibility to study reaction products in situ, i.e., without pressure quenching and to heat to very high temperature, therefore allowing to work in the thermodynamically controlled regime.

A rational approach to stabilize $[CN_3]^{5-}$ anions is to use counter-cations, which may possess oxidation states +5 in the absence of stable binary nitrides to favor the formation of ternary compounds. Following this rational design, in this work we synthesized antimony guanidinate $SbCN_3$ in a laser-heated DAC in three independent experiments in a pressure range 32–38 GPa (Table 1). Complete experimental details are provided in the Supporting Information.

Two of the three syntheses were performed from elements. A piece of Sb was placed on a diamond culet and the sample chamber was filled with nitrogen, which served as both a pressure medium and a reactant. The DACs were compressed to target pressures and then the Sb piece was heated by an infrared laser with an initial goal to obtain binary Sb nitrides. The heating products were then studied by means of synchrotron X-ray diffraction at ESRF (ID15b and ID27) and DESY (P02.2). Initial heating at ≈20 GPa did not result in any chemical reaction. We merely observed the recrystallization of Sb with the formation of the Sb-III (*bcc*) phase.[29] Reheating the sample at 32 GPa resulted in the emergence of sharp reflections on the X-ray diffraction images originating from multiple single-crystalline grains of the novel phases. Single-crystal diffraction datasets were analyzed using the well-established procedures for the treatment of multigrain samples[6,30] with the help of the newly-developed program, DaFi (Figures S1, S2, Table S2).[31]

The diffraction patterns of several prominent grains could be indexed with the rhombohedrally-centered hexagonal unit cell with a, $b=4.6040(3)$ Å and $c=13.9166(15)$ Å for one of such grains at 32.7 GPa. Initial structure solution and refinement revealed the chemical formula of the new compound as SbN_4, which is isostructural to $CaCO_3$ in the calcite modification (space group No. 167 $R\bar{3}c$), with Sb occupying the Wyckoff site 6*b* and N-atoms—Wyckoff sites 6*a* and 18*e*. Consequently, the proposed structure contained planar NN_3 anions. This NN_3-star anion has not yet been detected in a solid phase, but theoretical calculations predict this anion in several binary nitrides (ZnN_2, MgN_2, FeN_2).[32,33]

However, the experiment design does not preclude the involvement of carbon in the chemical reaction with Sb, raising the possibility that carbon atoms could reside at the center of the triagonal planar units. Indeed, the substitution of the central nitrogen atom of the NN_3 unit by carbon slightly decreases R_1 and wR_2 in the best crystal structure refinements (Table S3), thereby suggesting the chemical formula of the new compound to be $SbCN_3$ (Figure 1). Moreover, guanidinate anion $[CN_3]^{5-}$ perfectly satisfies the charge balance in $SbCN_3$, where Sb has an oxidation state of +5.

Table 1: Summary of the laser-heating experiments performed in DACs and their reaction conditions for the synthesis of $SbCN_3$.

Experiment	Reagents	Pressure (GPa)
1st	$Sb+N_2+C_{Dia}$	32.8
2nd	$Sb+N_2+C_{Dia}$	32.7
3rd	$Sb+C_3N_{12}$	38.0

In order to get a deeper insight into the stability of $SbCN_3$ we performed theoretical calculations within the framework of the density functional theory (DFT). The relative stability of $SbCN_3$ with respect to SbN_4 at 32 GPa was evaluated in the athermal limit by computing the reaction enthalpy of the reaction $SbCN_3+1/2\,N_2=SbN_4+C$, where $SbCN_3$ and SbN_4 had the calcite structure, C was in the diamond ($Fd\bar{3}m$) structure and N in the ε-phase ($R\bar{3}c$). The reaction is endothermic with calculated $\Delta H\approx 200$ kJ/mol. At 32 GPa, $SbCN_3$ is more stable than a mechanical mixture of Sb ($Im\bar{3}m$), diamond, and ε-N_2 ($R\bar{3}c$), while SbN_4 is less stable by 67 kJ/mol than a mixture of Sb and ε-N_2. Therefore, we conclude that due to the high thermodynamic stability of $SbCN_3$, carbon from the diamond anvil served as one of the reagents. Such synthesis approach appeared to be reproducible. Experiment #2 resulted in the same product, which was again confirmed by single-crystal X-ray diffraction (Table S2).

To enhance the synthesis strategy, in experiment #3 we have used cyanuric triazide (C_3N_{12}) as a precursor of carbon and nitrogen for the synthesis of $SbCN_3$. In this experiment no pressure-transmitting medium was used, while the Sb piece was positioned between the layers of C_3N_{12} in a DAC, preventing direct contact between Sb and the diamond culet.

Caution: Since energetic cyanuric triazide compound is to some extent unstable against external stimuli, proper safety precautions should be taken especially when handling the materials in amounts exceeding those, which are typically used for an experiment in a DAC. Lab personnel should wear protective equipment like grounded shoes, leather coat, Kevlar gloves, ear protection and face shields.

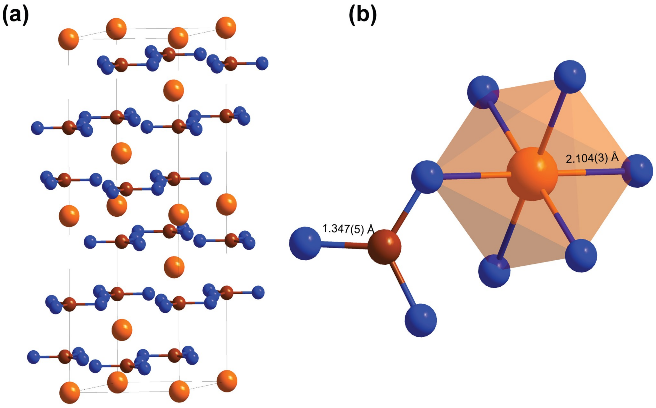

Figure 1. (a) Crystal structure of rhombohedral $R\bar{3}c$ calcite-type $SbCN_3$ at ambient pressure (0.0001 GPa). (b) The repeating $[SbN_6]$—octahedral units share one corner N - atom with planar triangular $[CN_3]^{5-}$ units. Sb, C and N atoms are shown in orange, brown and blue respectively.

Laser-heating at 38 GPa again resulted in the formation of $SbCN_3$ as evidenced by single-crystal and powder X-ray diffraction (Table S2, Figure S3). In this experiment we were able to decompress the DAC to ambient conditions and perform single-crystal X-ray diffraction data collection on the sample at 0.0001 GPa (Figure 2, S1, S2). To the best of our knowledge, $SbCN_3$ is the first example of a fully deprotonated guanidinate ever synthesized.

As at higher pressures, at 1 bar $SbCN_3$ is isostructural to calcite with $a=4.7305(3)$, $c=14.8134(13)$ Å.[34] The structure consists of planar triangular $[CN_3]^{5-}$ units coordinated to Sb cations via N atoms, forming slightly distorted SbN_6 octahedra (Figure 1). All direct Sb–N distances are 2.104(3) Å and covalent C–N bonds are 1.347(5) Å. In addition, all the N–C–N angles of the $[CN_3]^{5-}$ unit are 120° and the angles of N–Sb–N are close those of a regular octahedron. The distances are in a good agreement with theoretical calculations for $[CN_3]^{5-}$ units[26] as well as for Sb–N distances in octahedral coordination.[35]

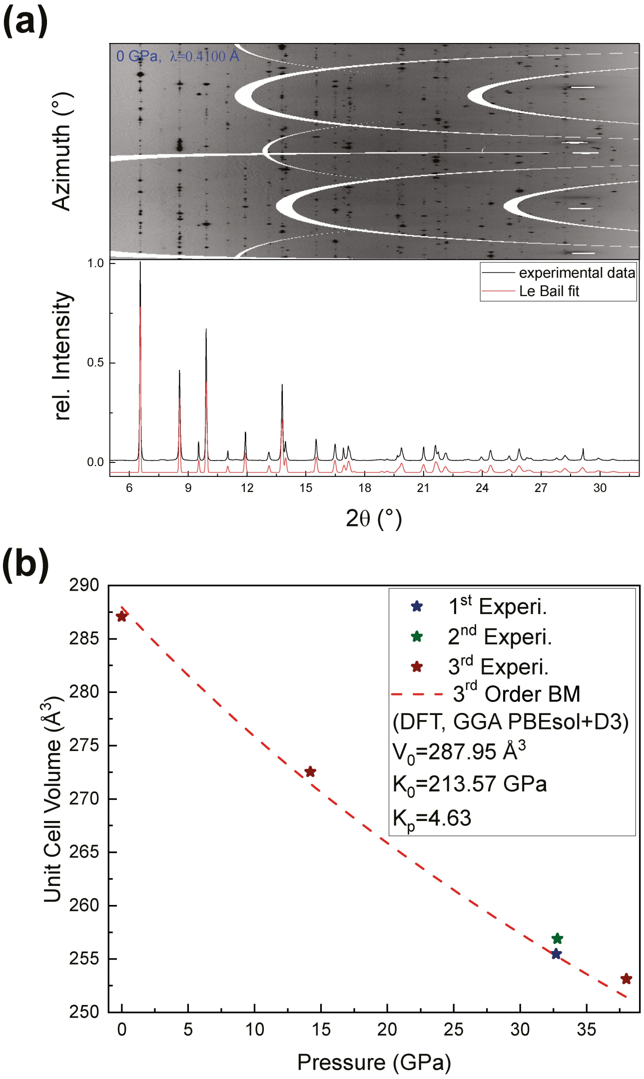

Figure 2. (a) Azimuthal integrated X-ray diffraction scan, powder diffraction pattern, and Le Bail fit from multigrain $SbCN_3$ at ambient pressure. (b) Calculated equation of state compared to the experimental unit cell volumes of $SbCN_3$. Experimental data can be used to determine the parameters of the second order Birch-Murnaghan equation of state with $V_0=287.5(11)$ Å^3, $K_0=228(10)$ GPa, $K'=4$ (fixed).

The experimental lattice parameters show very close agreement with our DFT calculations performed by using various levels of generalized gradient approximations (GGA) functionals, as shown in Table S5 (all details on theoretical calculations are provided in the Supporting Information). The experimentally generated and calculated pressure-volume data were used to determine the parameters of the 3rd-order Birch-Murnaghan equation of state.[36] The resulting equilibrium cell volume $V_0=287.95$, bulk modulus $K_0=213.56$ GPa, and its derivative with respect to pressure $K_0'=4.63$ are shown in Figure 2b. Due to higher formal ionic charges and, therefore, stronger bonding, the material is significantly more incompressible than isostructural carbonates.[37] The compressional behavior of $SbCN_3$ is anisotropic (Figure S4), which is also typical for rhombohedral carbonates due to quasi-layered structure.[37] The calculated elastic stiffness tensor demonstrates mechanical stability of $SbCN_3$ with $c_{11}=442(3)$, $c_{33}=260.6(8)$, $c_{44}=112.8(12)$, $c_{12}=114.5(17)$, $c_{13}=79.96(40)$, $c_{14}=18.4(4)$ GPa (Table S6). The phonon dispersion relations calculated in the harmonic approximation using DFT calculations confirm the dynamic stability of $SbCN_3$ both at ambient pressure, 0.0001 GPa, and at its synthesis pressures, 38 GPa, respectively, as shown in Figure S5.

Figure 3 shows the view of the electron localization function (ELF) by taking a slice through the planar $[CN_3]$ triangular units from the total ELF. The ELF shows that electron density in $SbCN_3$ is mainly localized on the N atoms. Bader charge analysis[38] (Table S7) shows that the Sb atoms act as a source of electrons for the N atoms in $SbCN_3$ with a substantial positive charge of $+2.80|e|$ on Sb atoms, and $-1.35|e|$ on N atoms, respectively, while a positive charge of $+1.27|e|$ on C atoms at ambient pressure.

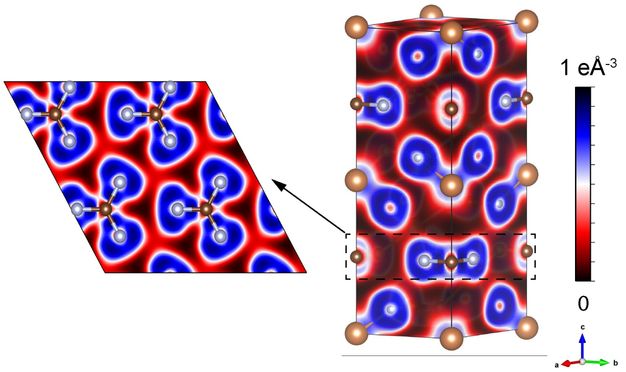

Figure 3. Electron localization function (ELF) demonstrates the localization of the electron density mainly around the N-atoms. On the left shown is the view of ELF sliced through the $[CN_3]$ units. Sb, C and N atoms are shown in orange, brown and light blue respectively.

Figure 4a shows the band structure of $SbCN_3$ at ambient pressure calculated using the GGA PBESOL+D3 functional. A direct band gap ($E_g = 0.94$ eV) occurs at the Γ—point of the Brillouin zone (BZ). As GGA functionals are known to underestimate the band gap in semiconductors, we also calculated the band gap using hybrid HSEsol functional and found it to be direct at the Γ—point of the BZ with the value $E_g = 2.20$ eV. Figure 4b shows the orbital-projected electronic density of states (eDOS). The occupied states are mainly from the N *p*-orbitals, whereas the unoccupied states are mainly dominated by the Sb *s*-orbitals. The valence band maximum (VBM) around the Γ—point is consisting of two-hole bands: heavy-hole (HH), and light-hole (LH), whereas the conduction band minimum (CBM) comprises of a sharp parabolic dispersion of electron band. Table S8 summarizes the calculated band gap values using the GGA and hybrid (HSEsol) functionals together with the effective mass of electron/hole states along different reciprocal direction of the crystal momentum in the BZ.

The occurrence of a direct semiconducting band gap certainly makes this material interesting for its potential use in optical and electronic devices. Therefore, we calculated the lowest-energy exciton binding energy of $SbCN_3$ in the context of semiclassical Mott-Wannier (MW) hydrogenic model.[39] In this model the exciton binding energy for a hydrogen-like state in a bulk semiconductor is expressed by the relation $E_b^{3D} = Ry(H).\mu_{ex}/m_0\varepsilon^2$, where Ry(H) = Rydberg constant = 13.6 eV is the ground state energy of a hydrogen atom, $\mu_{ex} = m_e m_h/(m_e + m_h)$ is the exciton reduced mass, m_0 is the rest mass of electron, and ε is the relative static dielectric constant. For simplicity, here we use the average effective hole mass for the light-holes (LH), 0.56 m_0 and the corresponding heavy-holes (HH), 1.32 m_0 from the Table S8 calculated from the curvatures of the energy bands. The static dielectric constant is given by $\varepsilon = \frac{2}{3}\varepsilon_{11} + \frac{1}{3}\varepsilon_{33}$, where the transverse ($\varepsilon_{11} = \varepsilon_{22}$) and lateral ($\varepsilon_{33}$) component of the macroscopic static dielectric tensors for $SbCN_3$ at ambient pressure were calculated using the density functional perturbation theory, including the local field effects in DFT using VASP, and found to be $\varepsilon_{11} = 8.52\varepsilon_0$ and $\varepsilon_{33} = 5.66\varepsilon_0$, respectively. The exciton binding energy calculated using the MW-model is found to be 46.48 meV using the average effective LH mass, and 58.06 meV using the average HH mass, respectively.

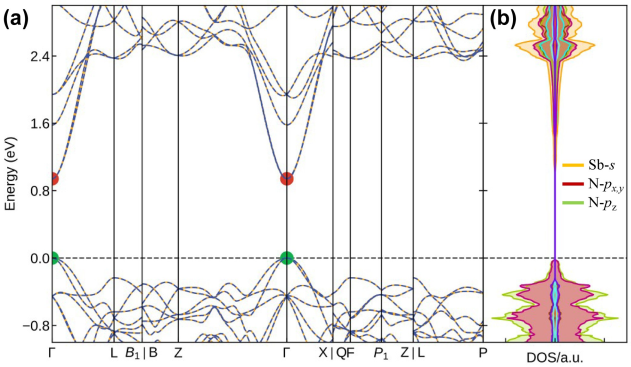

Figure 4. (a) Electronic band structure of $SbCN_3$ at ambient pressure 0.0001 GPa calculated using GGA (PBEsol + D3) functional. The direct band gap occurs at the Γ—point of the Brillouin zone (BZ). The value of the band gap calculated with more accurate hybrid HSEsol functional, $E_g = 2.20$ eV. (b) Orbital projected spin-polarized electronic density of states (eDOS) for $SbCN_3$ at ambient pressure. The occupied states are mainly from the N *p*-orbitals, whereas the unoccupied states are mainly arising from the Sb *s*-orbitals and a smaller contribution from C p_z-orbitals.

The exciton binding energy of $SbCN_3$ is comparatively higher than that of common semiconductors like bulk Si (14.3 meV)[40], and GaN (28 meV).[41] Therefore, a relatively high value of exciton binding energy in $SbCN_3$ is promising for enhanced electron-hole interactions that can lead to strongly coupled excitons which are useful for efficient excitonic emissions.

Figure S9a shows the optical absorption spectra as a function of incident photon energy in $SbCN_3$ at ambient pressure. A strong optical absorption in the visible part of the electro-magnetic spectrum (1.6–3.1 eV) makes this material interesting for light emitting diode, semiconductor laser, and solar cell applications. One can also expect a high charge-carrier mobility in this system owing to its small effective carrier masses at the CBM/VBM band edges near the Γ—point of the BZ.

To conclude, with this experiment we have resolved one of the long-standing chemical challenges—synthesis of fully deprotonated guanidinate anion $[CN_3]^{5-}$. This opens a route to the entire new family of inorganic carbonitrides. We can speculate that similar synthesis strategy and rational design may be applicable to the synthesis of orthonitridocarbonates $[CN_4]^{8-}$, analogous to orthocarbonates like M_2CO_4 (M=Mg, Ca, Sr, Ba).[13–15] During the preparation and production of this manuscript we became aware of the similar synthesis of oxoguanidinates of *f*-block metals,[42] which demonstrates the universality of high-pressure approach for the preparation of novel nitridocarbonates.

Acknowledgements

M.B. acknowledges the support of Deutsche Forschungsgemeinschaft (DFG Emmy-Noether Program project BY112/2-1). E.B. acknowledges the support of Deutsche Forschungsgemeinschaft (DFG Emmy-Noether project No. BY 101/2-1). N.J., I.A.A. acknowledge support by the Knut and Alice Wallenberg Foundation (Wallenberg Scholar grant no. KAW-2018.0194). Support from the Swedish Research Council (VR) grant no. 2019-05600 and the Swedish Government Strategic Research Areas in Materials Science on Functional Materials at Linköping University (Faculty Grant SFO-Mat-LiU no. 2009 00971) is gratefully acknowledged. DFT calculations were enabled by resources provided by the National Academic Infrastructure for Supercomputing in Sweden (NAISS) at National Supercomputer Center partially funded by the Swedish Research Council through grant agreement no. 2022-06725. B.W. is grateful for support through the Biovia Science ambassador program. We acknowledge DESY (Hamburg, Germany), a member of the Helmholtz Association HGF, for the provision of experimental facilities. Parts of this research were carried out at the beamline P02.2 of PETRAIII. Beamtime was allocated for proposal(s) I-11016188, I-20211466 and I-20221160. We acknowledge the European Synchrotron Radiation Facility (ESRF) for provision of synchrotron radiation facilities under proposal numbers MA5485, CH6476, CH6817. Open Access funding enabled and organized by Projekt DEAL.

Conflict of Interest

The authors declare no conflict of interest.

Data Availability Statement

The data that support the findings of this study are available in the supplementary material of this article.

Keywords: Antimony · Diamond Anvil Cell · High Pressure Synthesis · Nitridocarbonates · Single-Crystal X-Ray Diffraction

---

[1] C. Zhou, A. Ghods, V. G. Saravade, P. V. Patel, K. L. Yunghans, C. Ferguson, Y. Feng, B. Kucukgok, N. Lu, I. T. Ferguson, *ECS J. Solid State Sci. Technol.* **2017**, *6*, Q149–Q156.

[2] H. Wang, J. Li, K. Li, Y. Lin, J. Chen, L. Gao, V. Nicolosi, X. Xiao, J.-M. Lee, *Chem. Soc. Rev.* **2021**, *50*, 1354–1390.

[3] W. Sun, A. Holder, B. Orvañanos, E. Arca, A. Zakutayev, S. Lany, G. Ceder, *Chem. Mater.* **2017**, *29*, 6936–6946.

[4] M. Bykov, E. Bykova, A. V. Ponomareva, I. A. Abrikosov, S. Chariton, V. B. Prakapenka, M. F. Mahmood, L. Dubrovinsky, A. F. Goncharov, *Angew. Chem. Int. Ed.* **2021**, *60*, 9003–9008.

[5] M. Bykov, E. Bykova, G. Aprilis, K. Glazyrin, E. Koemets, I. Chuvashova, I. Kupenko, C. McCammon, M. Mezouar, V. Prakapenka, H.-P. Liermann, F. Tasnádi, A. V. Ponomareva, I. A. Abrikosov, N. Dubrovinskaia, L. Dubrovinsky, *Nat. Commun.* **2018**, *9*, 2756.

[6] M. Bykov, S. Chariton, H. Fei, T. Fedotenko, G. Aprilis, A. V. Ponomareva, F. Tasnádi, I. A. Abrikosov, B. Merle, P. Feldner, S. Vogel, W. Schnick, V. B. Prakapenka, E. Greenberg, M. Hanfland, A. Pakhomova, H.-P. Liermann, T. Katsura, N. Dubrovinskaia, L. Dubrovinsky, *Nat. Commun.* **2019**, *10*, 2994.

[7] M. Bykov, K. V. Yusenko, E. Bykova, A. Pakhomova, W. Kraus, N. Dubrovinskaia, L. Dubrovinsky, *Eur. J. Inorg. Chem.* **2019**, 3667–3671.

[8] K. Niwa, T. Yamamoto, T. Sasaki, M. Hasegawa, *Phys. Rev. Mater.* **2019**, *3*, 053601.

[9] K. Niwa, T. Terabe, D. Kato, S. Takayama, M. Kato, K. Soda, M. Hasegawa, *Inorg. Chem.* **2017**, *56*, 6410–6418.

[10] D. Laniel, B. Winkler, E. Koemets, T. Fedotenko, M. Bykov, E. Bykova, L. Dubrovinsky, N. Dubrovinskaia, *Nat. Commun.* **2019**, *10*, 4515.

[11] D. Laniel, M. Bykov, T. Fedotenko, A. V. Ponomareva, I. A. Abrikosov, K. Glazyrin, V. Svitlyk, L. Dubrovinsky, N. Dubrovinskaia, *Inorg. Chem.* **2019**, *58*, 9195–9204.

[12] X. Liu, P. Müller, P. Kroll, R. Dronskowski, *Inorg. Chem.* **2002**, *41*, 4259–4265.

[13] P. N. Gavryushkin, D. N. Sagatova, N. Sagatov, K. D. Litasov, *ACS Earth Sp. Chem.* **2021**, *5*, 1948–1957.

[14] V. Cerantola, E. Bykova, I. Kupenko, M. Merlini, L. Ismailova, C. McCammon, M. Bykov, A. I. Chumakov, S. Petitgirard, I. Kantor, V. Svitlyk, J. Jacobs, M. Hanfland, M. Mezouar, C. Prescher, R. Rüffer, V. B. Prakapenka, L. Dubrovinsky, *Nat. Commun.* **2017**, *8*, 15960.

[15] D. Spahr, J. Binck, L. Bayarjargal, R. Luchitskaia, W. Morgenroth, D. Comboni, V. Milman, B. Winkler, *Inorg. Chem.* **2021**, *60*, 5419–5422.

[16] R. Missong, J. George, A. Houben, M. Hoelzel, R. Dronskowski, *Angew. Chem. Int. Ed.* **2015**, *54*, 12171–12175.

[17] S. Benz, R. Missong, G. Ogutu, R. P. Stoffel, U. Englert, S. Torii, P. Miao, T. Kamiyama, R. Dronskowski, *ChemistryOpen* **2019**, *8*, 327–332.

[18] P. K. Sawinski, R. Dronskowski, *Inorg. Chem.* **2012**, *51*, 7425–7430.

[19] P. K. Sawinski, V. L. Deringer, R. Dronskowski, *Dalton Trans.* **2013**, *42*, 15080.

[20] G. Ogutu, E. Kozar, R. P. Stoffel, A. Houben, R. Dronskowski, *Z. Anorg. Allg. Chem.* **2020**, *646*, 180–183.

[21] V. Hoepfner, U. Englert, R. Dronskowski, *Z. Naturforsch. B* **2011**, *66*, 975–978.

[22] V. Hoepfner, P. Jacobs, P. K. Sawinski, A. Houben, J. Reim, R. Dronskowski, *Z. Anorg. Allg. Chem.* **2013**, *639*, 1232–1236.

[23] V. Hoepfner, R. Dronskowski, *Inorg. Chem.* **2011**, *50*, 3799–3803.

[24] A. L. Görne, J. George, J. Van Leusen, G. Dück, P. Jacobs, N. K. Chogondahalli Muniraju, R. Dronskowski, *Inorg. Chem.* **2016**, *55*, 6161–6168.

[25] A. L. Görne, J. George, J. van Leusen, R. Dronskowski, *Inorganics* **2017**, *5*, 10.

[26] D. Luo, X. Qiao, R. Dronskowski, *Angew. Chem. Int. Ed.* **2021**, *60*, 486–492.

[27] A. Zerr, G. Miehe, J. Li, D. A. Dzivenko, V. K. Bulatov, H. Höfer, N. Boifan-Casanova, M. Fialin, G. Brey, T. Watanabe, M. Yoshimura, *Adv. Funct. Mater.* **2009**, *19*, 2282–2288.

[28] X.-J. Chen, V. V. Struzhkin, Z. Wu, M. Somayazulu, J. Qian, S. Kung, A. N. Christensen, Y. Zhao, R. E. Cohen, H.-k. Mao, R. J. Hemley, *Proc. Natl. Acad. Sci. USA* **2005**, *102*, 3198–3201.

[29] D. Laniel, B. Winkler, T. Fedotenko, A. Pakhomova, S. Chariton, V. Milman, V. Prakapenka, L. Dubrovinsky, N. Dubrovinskaia, *Phys. Rev. Lett.* **2020**, *124*, 216001.

[30] E. Bykova, *Single-Crystal X-Ray Diffraction at Extreme Conditions in Mineral Physics and Material Sciences*, University of Bayreuth **2015**.

[31] A. Aslandukov, M. Aslandukov, N. Dubrovinskaia, L. Dubrovinsky, *J. Appl. Crystallogr.* **2022**, *55*, 1383–1391.

[32] Y. Chen, X. Cai, H. Wang, H. Wang, H. Wang, *Sci. Rep.* **2018**, *8*, 10670.

[33] S. Wei, D. Li, Z. Liu, X. Li, F. Tian, D. Duan, B. Liu, T. Cui, *Phys. Chem. Chem. Phys.* **2017**, *19*, 9246–9252.

[34] Deposition number 2280733 contains the supplementary crystallographic data for this paper. These data are provided free of charge by the joint Cambridge Crystallographic Data Centre and Fachinformationszentrum Karlsruhe Access Structures service.

[35] K. N. Heinselman, S. Lany, J. D. Perkins, K. R. Talley, A. Zakutayev, *Chem. Mater.* **2019**, *31*, 8717–8724.

[36] F. Birch, *Phys. Rev.* **1947**, *71*, 809–824.

[37] J. Zhang, R. J. Reeder, *Am. Mineral.* **1999**, *84*, 861–870.

[38] M. Yu, D. R. Trinkle, *J. Chem. Phys.* **2011**, *134*, 064111.

[39] J. Tilchin, D. N. Dirin, G. I. Maikov, A. Sashchiuk, M. V. Kovalenko, E. Lifshitz, *ACS Nano* **2016**, *10*, 6363–6371.

[40] A. J. Read, R. J. Needs, K. J. Nash, L. T. Canham, P. D. J. Calcott, A. Qteish, *Phys. Rev. Lett.* **1992**, *69*, 1232–1235.

[41] M. Dvorak, S.-H. Wei, Z. Wu, *Phys. Rev. Lett.* **2013**, *110*, 016402.

[42] A. Aslandukov, P. L. Jurzick, M. Bykov, A. Aslandukova, A. Chanyshev, D. Laniel, Y. Yin, F. I. Akbar, S. Khandarkhaeva, T. Fedotenko, K. V. Glazyrin, S. Chariton, V. B. Prakapenka, F. Wilhelm, A. Rogalev, D. Comboni, M. Hanfland, N. Dubrovinskaia, L. Dubrovinsky, *Angew. Chem. Int. Ed.* **2023**, *62*, e202311516.

Manuscript received: August 8, 2023
Accepted manuscript online: September 30, 2023
Version of record online: October 13, 2023